PAN
ARCHIVES OF ACOUSTICS
Vol. **44**, No. 1, pp. 117–127 (2019)
DOI: 10.24425/aoa.2019.126358

Theory of Synthesis of Asymmetrical Delay Line with the Surface Acoustic Wave

Milan ŠIMKO(1), Miroslav GUTTEN(1), Milan CHUPÁČ(1), Matej KUČERA(1)
Adam GLOWACZ(2), Eliasz KANTOCH(3), Hui LIU(4), Frantisek BRUMERCIK(5)

(1) *Department of Measurement and Application Electrical*
Faculty of Electrical Engineering, University of Žilina
Univerzitná 1, 010 26 Žilina, Slovakia
e-mail: {milan.simko, miroslav.gutten, milan.chupac, matej.kucera}@fel.uniza.sk

(2) *Department of Automatic Control and Robotics*
Faculty of Electrical Engineering, Automatics, Computer Science and Biomedical Engineering
AGH University of Science and Technology
Al. A. Mickiewicza 30, 30-059 Kraków, Poland
*Corresponding Author e-mail: adglow@agh.edu.pl

(3) *Department of Biocybernetics and Biomedical Engineering*
Faculty of Electrical Engineering, Automatics, Computer Science and Biomedical Engineering
AGH University of Science and Technology
Al. A. Mickiewicza 30, 30-059 Kraków, Poland; e-mail: kantoch@agh.edu.pl

(4) *College of Quality and Safety Engineering*
China Jiliang University
Hangzhou 310018, China; e-mail: liuhui2003@126.com

(5) *Department of Desing and Machine Elements*
Mechanical Engineering Faculty, University of Žilina
Univerzitná 1, 010 26 Žilina, Slovakia; e-mail: frantisek.brumercik@fstroj.uniza.sk

(*received November 17, 2017; accepted September 27, 2018*)

The aim of this publication is to design a procedure for the synthesis of an IDT (interdigital transducer) with diluted electrodes. The paper deals with the surface acoustic waves (SAW) and the theory of synthesis of the asymmetrical delay line with the interdigital transducer with diluted electrodes. The authors developed a theory, design, and implementation of the proposed design. They also measured signals. The authors analysed acoustoelectronic components with SAW: PLF 13, PLR 40, delay line with PAV 44 PLO. The presented applications have a potential practical use.

Keywords: delay line; diluted electrodes; surface acoustic wave; interdigital transducers; resonators.

1. Introduction

Among the perspective acoustoelectronic components with the surface acoustic waves (SAW) there are the bandpass filters, delay lines (DL), and resonators, which are used as selective elements of oscillators with harmonic oscillations (Nevesely, 1986; Hartmann, 1985; Ruppel, Fjeldy, 2000). The main advantage is their small size and low weight, high mechanical strength, low sensitivity to vibration as well as the possibility to make the oscillators without the use of inductor. This is what guarantees their manufacturing perspective and wide range of use in measuring of electric and non-electric variables, in radio electronics, telecommunications, and introduces the necessity of elaboration of questions concerning their theory and manufacturing.

According to the literature, delay lines can be realised by electrical or acoustic means (Hasanov, Hasanov, 2017; Kim *et al.*, 2017; Zhu, Rais-Zadeh,

2017; Alshaykh *et al.*, 2017; Audier *et al.*, 2017; Marzo *et al.*, 2017; Young *et al.*, 2017; Cheng *et al.*, 2017; Gruber *et al.*, 2016; Djoumi *et al.*, 2016; Zhang, Hu, 2015; Tung *et al.*, 2015; Zheng *et al.*, 2015). The SAW delay line is used instead of transmission systems composed of a few thousands of transistors.

In the present paper the authors develop a theory of an asymmetrical delay line with interdigital transducer (IDT) with diluted electrodes.

2. Synthesis of asymmetrical delay line

An asymmetrical delay line has an input IDT with a small number of electrodes (i.e. broadband), and an output IDT with a large number of electrodes (i.e. narrowband). Module characteristic can be close to the synchronous frequency sufficiently accurately approximated by the function of

$$\frac{\sin x}{x}, \qquad \text{where} \quad x = N\pi\frac{(f-f_0)}{f_0}.$$

When increasing the number of electrodes IDT, however, there is a signal caused by reflections from the edges of the electrodes, which substantially impairs the delay line properties and at the same time of the whole oscillator. To suppress the signal the authors partly remove the electrodes in the narrowband IDT (i.e. "*diluted*" – divided into groups IDT). A similar problem arises in the synthesis of the filter with a narrow and very narrow pass band $\Delta f_3/f_0 = 0.1$ to 0.5% (n. On the contrary, the methods of synthesis of filters with SAW are accurate at a relatively wide pass band $f_3/f_0 = 1$ to 30%).

2.1. Frequency and time characteristics of the individual groups of electrodes in the IDT with diluted electrodes

The diluted IDT refers only to the periodic removal of the same groups of electrodes of IDT (Fig. 1a). If there is a change of the period or distance of groups and also the number, overlap, step, width, or other parameter of electrodes of the retained groups according to a certain rule which differs from the one accepted in the original IDT, then we are talking about so called weighing of electrodes and it needs to be examined separately.

In the general case, if we do not consider the discretisation in the process of sampling time, the impulse characteristic of diluted IDT can be expressed in the form of the sum of the impulse characteristics $h_m(t-t_m)$ shifted for a period of T_r (Fig. 1b), i.e.

$$h_r(t) = \sum_{m=1}^{M} h_m(t-t_m), \tag{1}$$

where $h_m(t-t_m)$ is a function which describes the pulse characteristic of a group consisting of N_i pairs of unsplit electrodes with the length T_i, m is a group number, M is the number of groups, and $t_m = mT_r$.

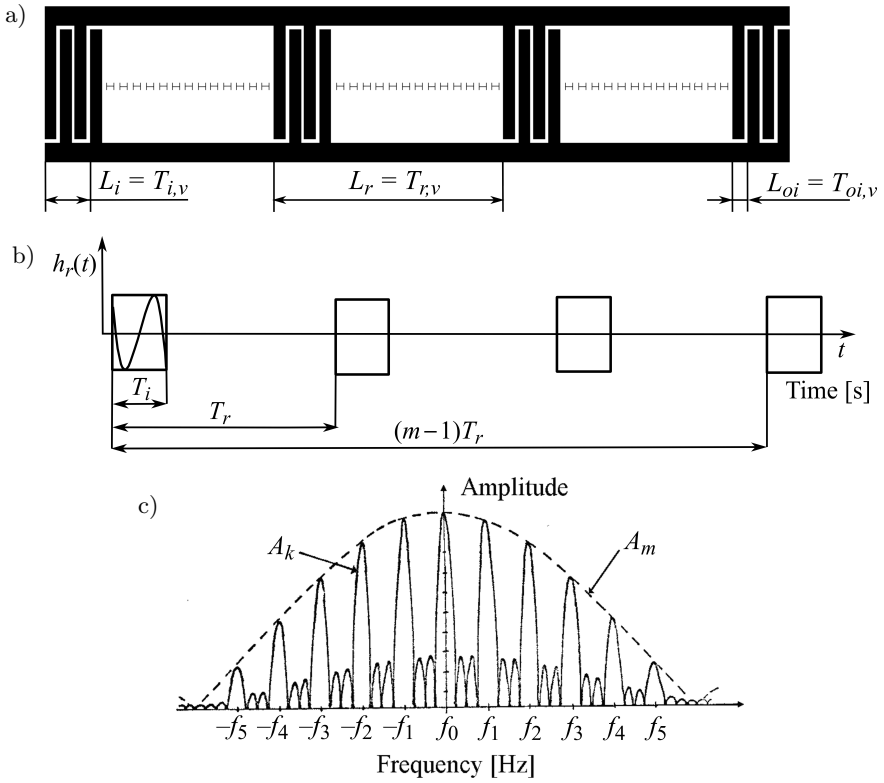

Fig. 1. IDT with periodically diluted electrodes.

A parameter $r = T_r/T_i$ is called substituting dilution, by analogy with the impulse modulation of signals.

In the special case of division into groups of an apodised IDT where $a(t)$ is the apodization function its impulse characteristics has the shape

$$h_r(t) = \sum_{m=1}^{M} a(t) h_{mr}(t - t_m), \tag{2}$$

where

$$h_{mr} = \begin{cases} 1 \text{ for } (m-1)T_r \le t \le (m-1)T_r + T_i, \\ 0 \text{ for } (m-1)T_r + T_i \le t \le mT_r, \end{cases}$$

is a periodic sequence of the impulse characteristics of groups with the same aperture.

According to linear properties of Fourier transformation, the transfer function of the IDT with diluted electrodes represents a convolution of the transfer function $H_{mr}(j\omega)$ of the undiluted IDT and of the spectrum of modulation function $H_a(j\omega)$ of group and is equal to the sum of the spectra of the individual groups that are repeated with the repetition rate $f_r = 1/T_r$.

It uses the following Eq. (3):

$$H_r(j\omega) = \sum_{m+1}^{M} A_m(\omega) \mathrm{e}^{j\Theta m^{(\omega)}} = H_{mr}(j\omega) * H_a(j\omega), \tag{3}$$

where $A_m(j\omega)$ is module characteristics of the m-th group, $\Theta_m(\omega) = \Theta_{mr}(\omega) + \Theta_{mn}(\omega)$ is argument characteristics of the m-th group, $\Theta_{mr}(\omega)$ is the initial phase of the group which is determined by the control period T_r, $\Theta_{mn}(\omega)$ is the phase change within the group.

In the periodic dilution, due to removing of electrodes within the length of the whole transducer, the phase shift of each group in the synchronous frequency is ω_0 times π and the initial phase of the m-th group, $\Theta_{mn}(\omega_0) = \omega_0 T_m = \omega_0 (m-1) T_r = \pi (m-1) N_r N_i$, where $T_m = (m-1) T_{0i} N_i r$ is the time coordinate of the edge of the m-th group with the respect to the edge of the transducer, $N_r = N_i r$ is the number of electrode pairs attributable to the spatial period L_r (Fig. 1a), $T_{0i} = 1/(2f_{0i})$ is the period of location of the unsplit electrodes of the i-th group.

Let us examine the characteristics of one of non-apodised group with equidistant distribution of electrodes. If we do not consider discretisation of impulse characteristics in the process of sampling time, the equation for the transfer function $H_{mr}(j\omega)$ group is analogous to the equation for the spectral density of videoimpulse T_i. When reading from the edge of the group ($0 \le t \le T_i$), the equation in a wide frequency range of $0 \le \Omega \le \Omega_N$ has the shape

$$H_{mr}(j\omega) = \frac{1}{j\Omega} \left(1 - \mathrm{e}^{-j\Omega T_i}\right) = \frac{2}{\Omega} \sin\left(\frac{\Omega T_i}{2}\right) \mathrm{e}^{-j\Omega T_i/2}, \tag{4}$$

where $\Omega = \omega - \omega_0$, $\Omega_N = \omega_N - \omega_0$, ω_N is the Nyquist frequency.

From this equation the module characteristics can be expressed by the relation

$$A_m(\Omega) = \left| \frac{2}{\Omega} \sin \frac{\Omega T_i}{2} \right| \tag{5}$$

and the argument characteristics which is determined by the mutual spacing of electrodes, by the relation

$$\Theta_{mn}(\Omega) = \frac{\Omega T_i}{2} + (k-1)\pi \tag{6}$$

for

$$(k-1)\frac{2\pi}{T_i} \le \Omega \le (k+1)\frac{2\pi}{T_i},$$

where

$$k = 1, 2, 3, ..., \frac{\Omega_N}{T_i}.$$

In cases where readings are performed from the centre of a non apodised group ($-T_i/2 \le t \le T_i/2$), the transfer function of the group is given by the relation

$$H_{mr}(j\omega) = \frac{1}{j\Omega} \left(\mathrm{e}^{j\Omega T_i/2_i} - \mathrm{e}^{-j\Omega T_i/2}\right) = \frac{2}{\Omega} \sin\left(\frac{\Omega T_i}{2}\right), \tag{7}$$

from which

$$A_m(\Omega) = \left| \frac{2}{\Omega} \sin \frac{\Omega T_i}{2} \right| \tag{8}$$

and

$$\Theta_{mn}(\Omega) = (k-1)\pi \tag{9}$$

for

$$(k-1)\frac{2\pi}{T_i} \le \Omega \le (k+1)\frac{2\pi}{T_i},$$

where

$$k = 1, 2, 3, ..., \frac{\Omega_N}{T_i}.$$

It results from the above that the module characteristics of the non apodised group is of the same shape, independently from the beginning of reading and the argument characteristics is linear, angled at $0 \le t \le T_i$ and stepped at $-T_i/2 \le t \le T_i/2$.

If we use the model of functions δ, the impulse characteristics of the IDT, considering the discretisation, can be expressed by a sequence of functions δ located in the centre of electrodes. Therefore, the transfer function of the apodised equidistant group, which is symmetrical relative to the centre of readings, according to the properties of the IDT with the linear phase and considering Eq. (9) is expressed by the following Eq. (10):

$$H_{mr}(j\omega) = \left[1 + 2\sum_{n=1}^{N_i} (-1)^n \gamma_{ni} \cos(\omega n T_{0i})\right] \mathrm{e}^{-j(k-1)\pi} \tag{10}$$

for an odd number of electrodes in the group $A_i = 2N_i + 1$ and

$$H_{mr}(j\omega) = \left\{ j2 \sum_{n=1}^{N_i} (-1)^n \nu_{ni} \sin\left[\omega\left(n - 0.5\right) T_{0i}\right] \right\} \cdot \mathrm{e}^{-j[(k-1)\pi + (\omega_0 - \omega)T_i]/2} \tag{11}$$

for an even number of electrodes in the group $A_i = 2N_i$.

In Eqs (10) and (11), $k = 1, 2, 3, ..., \Omega_N/T_i$, γ_{ni} and ν_{ni} are coefficients of impulse characteristics of a group, T_{0i} is an interval of discretisation of the group. For a non apodised group $\gamma_{ni} = \nu_{ni} = 1, 0$. At a changing overlap of the electrodes, γ_{ni} and ν_{ni} vary according to the given rule.

In the previous analysis, the authors did not consider the interaction of electrodes of the IDT and the frequency dependence of the intensity of radiation of pair of electrodes forming an elementary group.

2.2. Transmission properties of the diluted IDT over a wide frequency range

For the non apodised equidistant IDT, which consists of M the same groups symmetrical relative to the centre, $\Theta_{mn}(\omega) = 2\pi$ and Eq. (3) can be simplified to the form

$$\begin{aligned} H_{mr} &= A_m(\Omega) \sin\left(\frac{\pi\omega}{2\omega_0}\right) \left[1 + \mathrm{e}^{-j\Omega T_r} + \mathrm{e}^{-j2\Omega T_r} + ... \right. \\ &\quad \left. + \mathrm{e}^{-j(m-1)\Omega T_r} + \mathrm{e}^{-j(M-1)\Omega T_r}\right] \\ &= A_m(\Omega) \sin\left(\frac{\pi\omega}{2\omega_0}\right) \sum_{m=1}^{M} \mathrm{e}^{-j(m-1)\Omega T_r}. \end{aligned} \tag{12}$$

At frequencies satisfying the condition $\Omega_k = k2\pi/T_r = k2\pi f_r$, each addend in square brackets equals one, and if we do not consider the frequency dependence of the radiation of electrodes, the transfer function will have the shape

$$H_r\left(\frac{k2\pi}{T_r}\right) = M A_m\left(\frac{k2\pi}{T_r}\right). \tag{13}$$

At frequencies $\Omega_k = k2\pi/T_r = k_2\pi f_r$ (or $f_k = f_0 \pm k/T_r = f_0 \pm k f_r$) the transfer function of the diluted IDT contains partial pass bands.

Thus, the module characteristics of the diluted IDT (Fig. 1c) has, in addition to a basic pass band at frequency f_0, partial pass-bands at frequencies $\pm f_k$, with "the step" f_r, which is inversely proportional to the spatial period L_r. The size of partial module characteristics $A_k(f)$ varies depending on the module characteristics of the group $A_m(f)$.

2.3. Use of the diluted interdigital transducers

The diluted IDT can be used for the construction of narrowband filters with comblike frequency response. In that case it is advantageous to use narrowband IDT_1 with diluted electrodes and broadband IDT_2. According to Eq. (3), the transfer function of the filter will have the range of narrowband partial passbands caused by dilution of electrodes of the IDT_1.

However, we require more often filters with one permeable band. Figure 2a shows schematically a narrowband filter consisting of the diluted IDT_1 and the broadband IDT_2. There are two possible variants of their arrangement. In the first one, the spatial periods L_1 and L_2 are the same, in the second one they are different ($L_1 < L_2$, $L_1 > L_2$, respectively). In a simple case it can be any group of the IDT_1 consisting of one pair of electrodes.

In the first case ($L = L_1 = L_2$), it must be for the suppression of partial passbands that the length of the IDT_2 is equal to the period of control of the $\mathrm{IDT}_1 - L_r$. If the condition is satisfied, the zeros of the module characteristics of the broadband IDT_2 (Fig. 2b) are identical with maximum values of partial passbands (except for the passband at f_0).

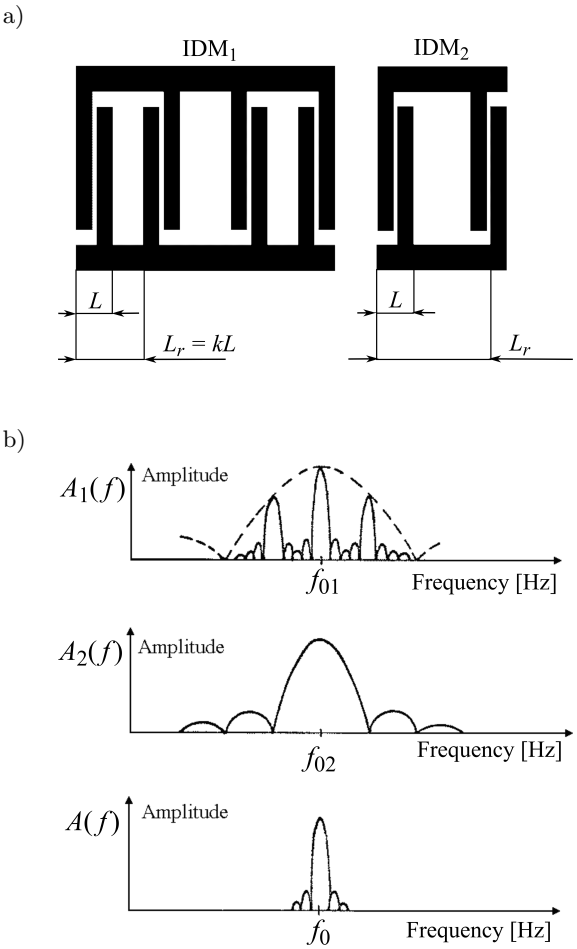

Fig. 2. IDT with diluted electrodes.

In the second case, for the suppression of partial passbands, the spatial period L_r must be a multiple of

the ratio of the product of L_1 and L_2 and the difference between these periods (Fig. 3a), i.e.

$$L_r = \frac{kL_1L_2}{L_1 - L_2}, \qquad \text{if} \quad L_1 > L_2, \tag{14}$$

and

$$L_r = \frac{kL_1L_2}{L_2 - L_1}, \qquad \text{if} \quad L_1 < L_2, \tag{15}$$

where k is an integer, $L_1 = v/(2f_{01})$, $L_2 = v/(2f_{02})$, and f_{01}, f_{02} are synchronous frequencies of IDT.

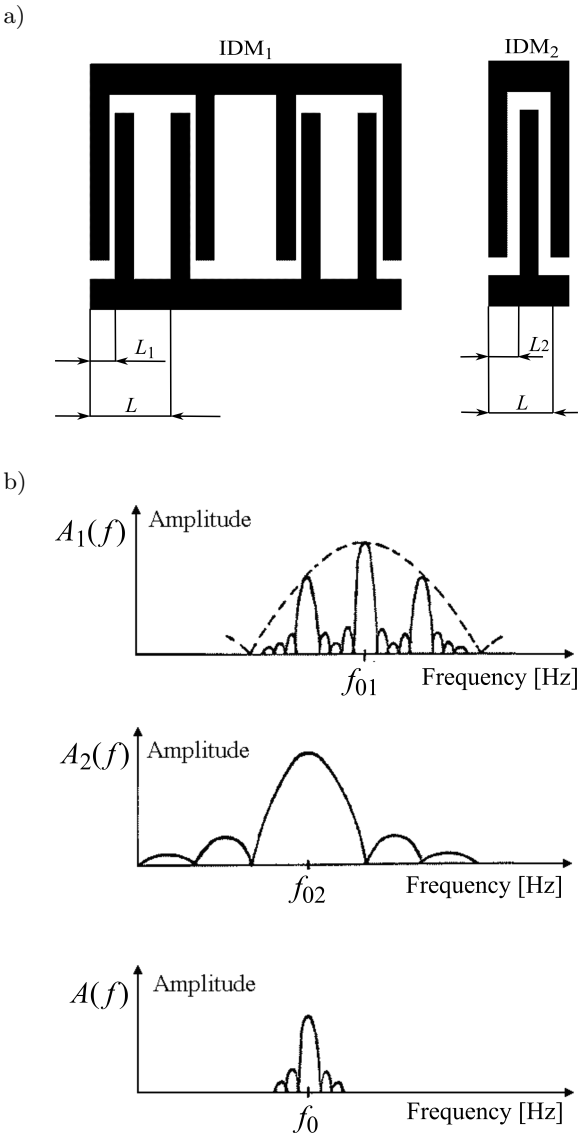

Fig. 3. IDT with diluted electrodes.

If the condition (14) is satisfied, the maximum of the module characteristics of IDT is equal to the k-th passband at the frequency $f_k = f_{01} + kf_r$ and while satisfying the condition (15) it is equal to the k-th passband at the frequency $f_k = f_{01} - kf_r$.

The passbands of the diluted IDT_1 are suppressed significantly except for the passband at the frequency f_k. For this reason, in Fig. 3b one passband $f_k = f_0 \pm kf_0 = f_{02}$ is presented.

Even narrower passband $\Delta f_3/f_0 = 0.1$–0.2% can be realised using two diluted IDTs (Fig. 4a). In this case, it is also possible to have two variants of narrowband filters construction. In the first variant there are the synchronous frequencies of both diluted IDT (or spatial periods of electrodes) being the same, i.e. $f_{01} = f_{02}$ a $L_1 = L_2$ and for the spatial periods of groups used for Eq. (16):

$$\frac{L_{ri}}{L_{r2}} = \frac{f_{r2}}{f_{r1}} = \frac{T_{r1}}{T_{r2}} = \frac{k}{l}. \tag{16}$$

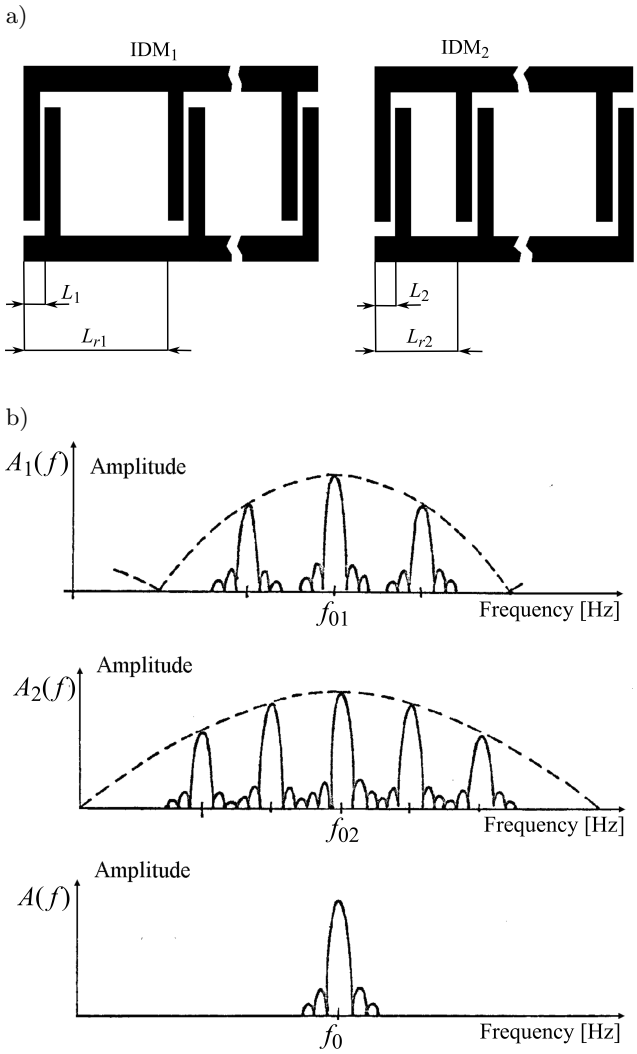

Fig. 4. Two diluted IDTs.

When this condition is satisfied, partial passbands of the IDT_1 at the frequency $f_k = f_{01} \pm kf_{r1}$ identify with partial passbands of the IDT_2 at the frequency $f_1 = f_{02} \pm lf_{r2}$ and in the resulting module characteristics of filter there is only one passband at the frequency $f_0 = f_k = f_1$ (Fig. 4b).

In the second variant, the spatial periods L_1 and L_2 are different (Fig. 5a), i.e. $L_1 > L_2$ or $L_1 < L_2$ and the

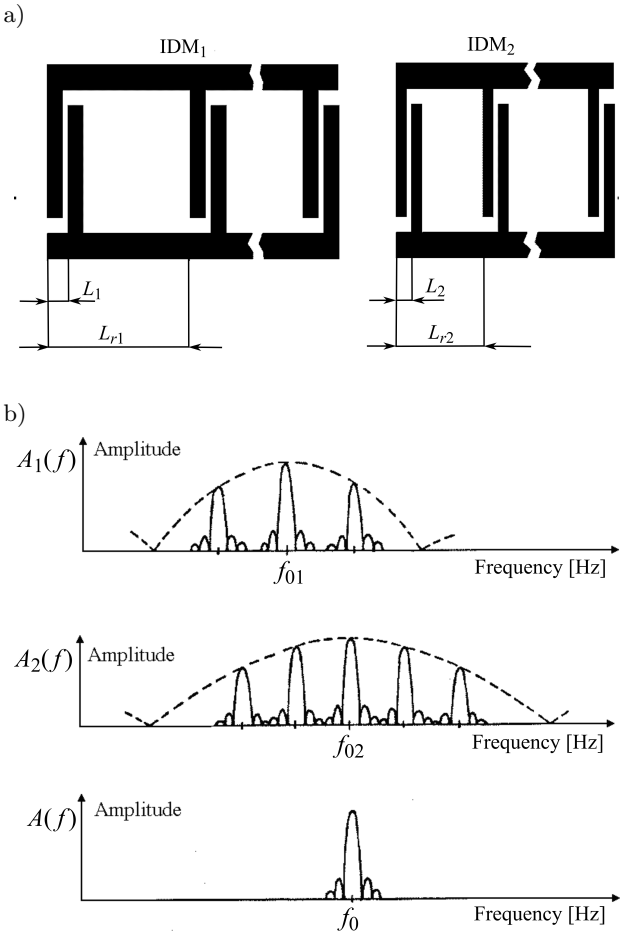

Fig. 5. Two diluted IDTs.

spatial period of groups of the first L_{r1} and second L_{r2} of IDT are an integer multiple of the wavelengths λ_1 and λ_2, corresponding to the synchronous frequencies f_{01} and f_{02} of these transducers and they are determined from the relation

$$\frac{L_{ri}}{L_{r2}} = \frac{L_{r1}\left(\frac{1}{L_1} - \frac{1}{L_2}\right)}{2l + \frac{k}{l}}, \tag{17}$$

where k and l are integers.

In the first case ($L_1 > L_2$) and in the second ($L_1 < L_2$) case, all improper identified partial passbands are significantly suppressed and belong to the resulting module characteristics of the filter. There is only one desired passband for a synchronous frequency $f_0 = f_k = f_1$ (Fig. 5b).

In these constructions of narrowband filters with two diluted IDTs, the operating range of filters can be extended: in the lower part to the values of 0.5 to 1 MHz and less, by using "low-frequency" partial passbands, and in the upper area to the values of 500 to 600 MHz, by using "high-frequency" partial pass bands, without increasing the dimensions of the filter and at the same time without increasing the requirements for the resolution of photolithography.

Construction of diluted IDTs enables retuning of the filter to a variety of synchronous frequencies easily. If metal strips are placed into the gaps between individual groups of diluted IDTs (Fig. 6a), by the change of the width of these strips we can change the speed of the propagation of SAW in the IDT and thus move the partial passband of one or other IDT, the left or right ones. At a certain speed of SAW, there will be identification of some partial pass bands so we can change synchronous frequency of the filter (Fig. 6b). The indicated design allows us to use one photomask to make a variety of different filters with different synchronous frequencies. (The width of the metal strip can be changed with the help of, e.g., chemical etching, laser, etc.).

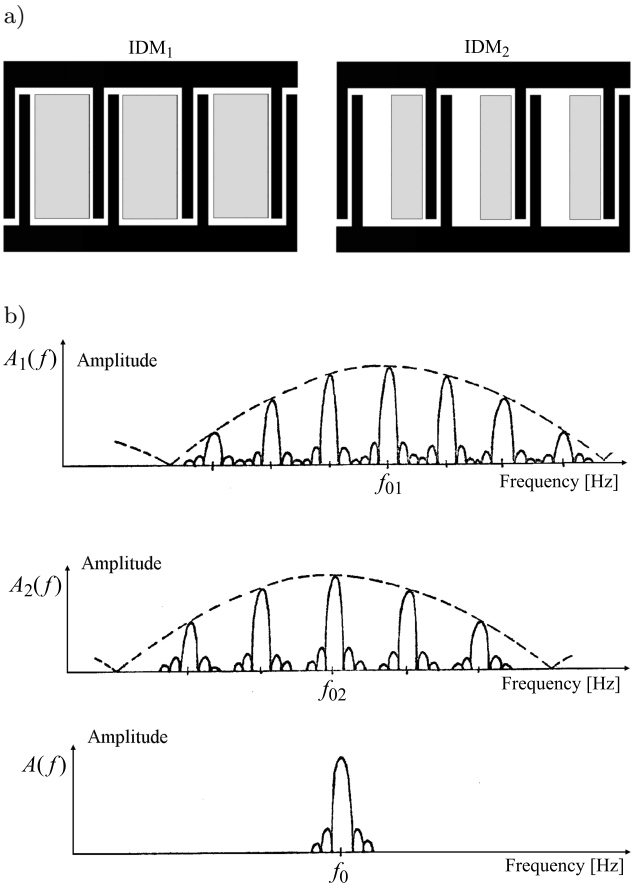

Fig. 6. Diluted IDM with a metal strip.

3. Experimental results

On the basis of the above theory the authors designed, implemented and experimentally verified a few filters and resonators for sensors of non electrical quantities. Below there is an example of the developed filter (it can be used, e.g., for oscillators of common TV distribution, etc.).

A PLF 13 filter has been designed and implemented using Fourier transformation and weighing functions.

Required parameters of PLF 13:

synchronous frequency – 143.5 MHz,
bandwidth "to 3 dB" is ± 14 MHz,
group delay – $T < 10$ ns.

Selected substrate:

Y – cut, Z – the direction of propagation $LiNbO_3$.

The filter contains the IDT_1 with diluted electrodes and the broadband IDT_2 with the same spatial period ($L_1 = L_2$). The diluted IDT_1 has 42.5 groups made up of one pair of electrodes, i.e. 85 electrodes. The broadband IDT_2 has 11 electrodes, i.e. 5.5 pairs. The spatial period: $L = \lambda_0/2 = 8$ µm, period of dilution: $L_r = 2500$ µm. Aperture: $w = 2300$ µm. Synchronous frequency of the filter $f_0 = 143.5$ MHz, the inserted damping: $b_d = 12$ dB, quality factor: $Q = 650$. The design of the implemented filter is shown in Fig. 7.

A temperature sensor was designed and implemented. One port resonator (Fig. 8) with the electrically shortcircuiting reflector system array PLR40 was used. It had a lower inserted damping. Thus for further signal processing we could use a single stage amplifier of the electrical signal. The calculated, measured parameters of the resonator and delay line are shown in Tables 1 and 2.

Table 1. Parameters of the implemented acustoelectronic components (calculated and measured).

Parameter	PLF 13	PLO 44	Remark
v_{ef} [pF/m]	3445	3445	
K^2	0.0482	0.0482	
C'_s [pF/m]	398.2	434.4	specific capacity of section
λ_0 [µm]	25	40	$\lambda_0 = v_{ef}/f_0$
$l_e = l_0$ [µm]	8	10	electrode and gap width
f_{oc} [MHz]	143.5	87.2	calculated
f_{oM} [MHz]	144.2	86.7	measured
N	85	11	
n	42	5	$n = 2N + 1$
l' [µm]	2125	440	$l = N\lambda_0$
l [µm]	5225	8650	$l = P_0\lambda_0$
P_0	≈ 250	≈ 250	
k	250	250	
C_{TC} [pF]	289	391	$C_T = C'_s wN$
C_{TM} [pF]	284	382	measured
Q_{C}	665	768	$Q = \pi P_0$
Q_{M}	≈ 650	≈ 780	measured
b_d [dB]	12	18	inserted damping
w [µm]	2300	3000	aperture

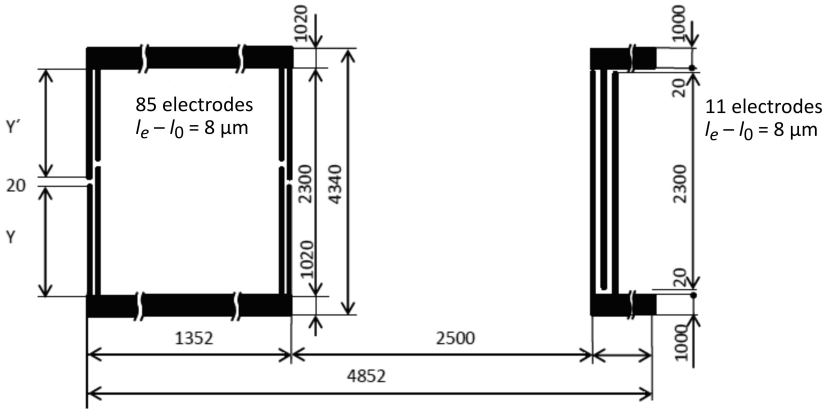

Fig. 7. Design of the produced filter.

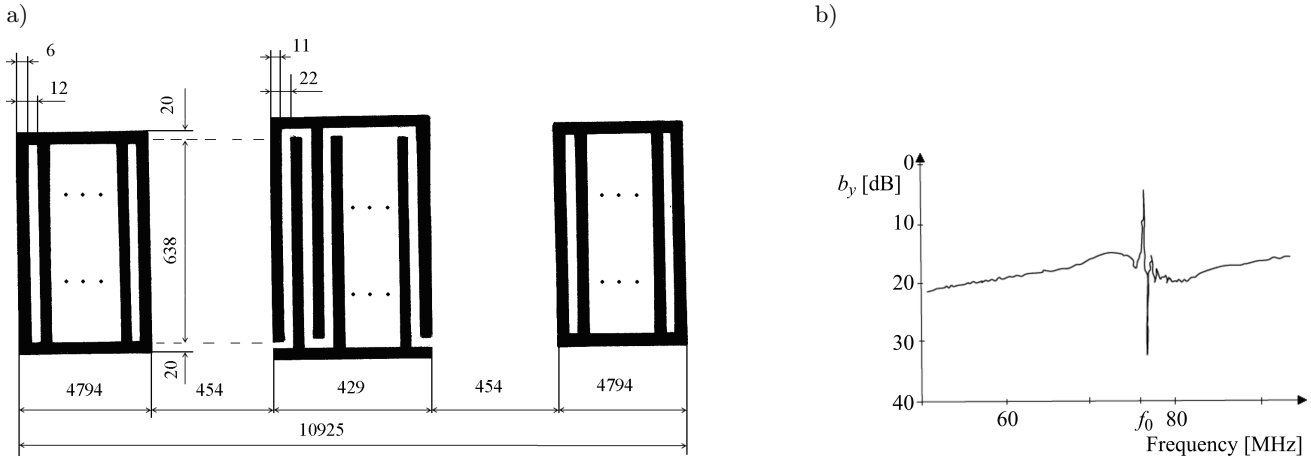

Fig. 8. One port resonator PLR 40.

Table 2. Parameters of implemented acustoelectronic components (calculated and measured).

Parameter	PLR 40	Remark
v_{ef} [pF/m]	3357	
K^2	0.0482	
C'_s [pF/m]	395.9	specific capacity of section
ε	–0.0241	impedance matching
$\|r\|$	0.948	the absolute value of the reflection coefficient
N	400	number of elements of the reflection system
d [mm]	2.39	distance of the apparent plane of reflection
m_d	70	
s [mm]	1.42	distance of the inner edges of the reflection systems
m_s	110	
R_1 [Ω]	29.64	equivalent circuit
L_1 [μH]	0.101	
C_1 [pF]	0.0401	
C_T [pF]	3.45	
R_T [Ω]	1148	
R_e [Ω]	10	
f_{ov} [MHz]	75.84	series resonance frequency – calculated
f_{oM} [MHz]	76.068	measured
f'_{ov} [MHz]	76.28	parallel resonance frequency – calculated
f'_{oM} [MHz]	76.324	measured
n_f	20	number of electrodes IDM
$l_e = l_0$ [μm]	11	electrode and gap width
w	638	aperture
Q_{sM}	2415	factor quality series resonance
Q_{pM}	2642	factor quality parallel resonance
C_{TM} [pF]	2.14	static kapacitance rezonator
b_d [dB]	10	inserted damping

Required parameters of PLR 40:

IDM: $N = 10$ electrode, $l_e = l_0 = 11$ μm.

Reflection system: $N = 400$ electrode, $l_e = l_0 = 6$ μm.

Selected substrate:

Y – cut, Z – the direction of propagation $LiNbO_3$, thickness of the pad – 0.5 mm.

Another actual example of the use of the developed theory was design and implementation of delay lines which have been used for the identification system with the SAW. It had advantages over other systems.

Example of an identification system using the properties of SAW is shown in Fig. 9. It consists of a transmitter, receiver, computer (i.e. evaluation unit), and passive identification card.

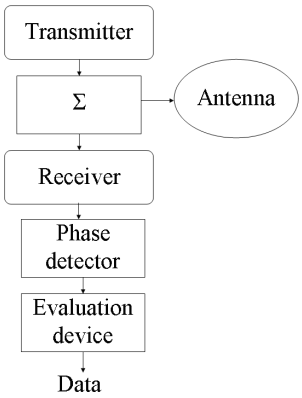

Fig. 9. Example of an identification system using the properties of SAW.

The identification card with the code number is located in the observation unit (e.g. a railway wagon, etc.) It can be identified remotely using an impulse transmission system. An impulse transmission system sends a short query high frequency signals to the identification card. Next, after a short delay, the card sends a coded response, which is recorded by the receiver with the phase detector. The transmitter sends short radio impulses with a certain carrier frequency (MHz), duration (typically 0.5 ± 0.1 μm) and repeated

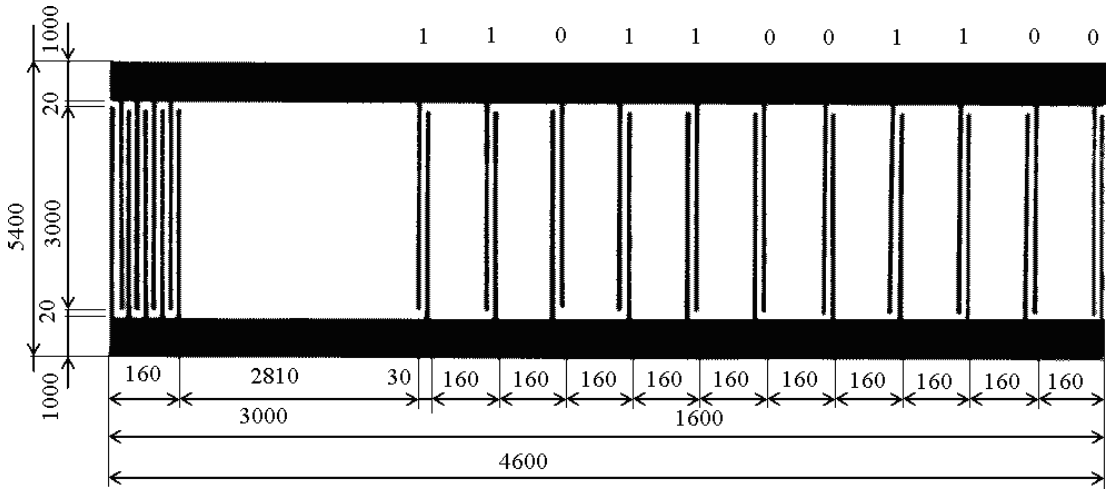

Fig. 10. Delay line PLO 44.

frequency (e.g. 3 Hz, etc.). The transmitter range is limited within a few meters (antenna radiation is narrowly directed). Next, the signal is processed in the evaluation unit.

A designed delay line PLO 44 (Fig. 10) consists of an input IDT_1 and an output IDT_2. The transducers are made by using photolithographic technology on the piezoelectric substrate cut Y, Z direction of propagation of the $LiNbO_3$. The two transducers and the loop antenna are connected together. The required selected number in the binary system is obtained by the phase modulation of the signal. The criterion of the design is that the length of the space period L_1 must be greater than the period of the length L_2. By increasing the number of pairs of electrodes it can be expanded by number of possible display numbers. (e.g. the first pair forms a so called start (trigger) bit, followed by a sequence of zeros and ones forming in the binary system a certain number, followed by control of parity, stop bit, etc.).

Required parameters PLO 44:

IDM: $n = 9$ electrodes, $l_e = l_0 = 10$ μm,
$n = 2$ electrodes, $l_e = l_0 = 10$ μm.

Selected substrate:

Y – cut, Z – propagation direction, $LiNbO_3$,
thickness of the pad – 1 mm, $f_0 = 87.2$ MHz.

It can be noticed that:

- An additional requirement for the topology of the filter with the single narrowband diluted IDT and the broadband IDT is maintaining the ratio of the spatial period of groups of the diluted IDT and the length of the broadband IDT. The ratio ensures the suppression of unwanted partial passbands of the module characteristics.
- There were introduced requirements for repetition accuracy of the spatial period of the electrodes and groups for filters with two diluted IDTs. In this way identification of partial passbands at a given frequency and suppression of unwanted pass bands can be fully secured.
- The developed theory of synthesis can be advantageous for both described structural variants of filters, operating on various partial passbands. It can be also used for design and realisation of a wide range of acoustoelectronic components with SAW.
- The proposed theory was used for narrowband filters, delay lines for the single mode oscillators, and resonators.
- The results of the conducted analysis are essential for the development of knowledge in the given scientific field and applications of acoustoelectronic components.
- The authors presented realisation of the acoustoelectronic components.

4. Conclusions

The paper also deals with the surface acoustic waves (SAW) and the theory of synthesis of the asymmetrical delay line with the interdigital transducer with diluted electrodes. The authors developed a theory, design, and implementation of the proposed design. The authors also carried out measurements.

The authors analysed acoustoelectronic components with SAW: PLF 13, PLR 40, delay line with PAV 44 PLO. The filter PLF 13 was used for the oscillator of common television distribution. One port of the resonator PLR 40 was used for application of the temperature sensor (10 dB). The temperature sensor developed on the basis of the delay line has a high attenuation (52 dB). It was necessary to use a multistage amplifier. Next, the delay line and PAV 44 PLO were described and used in the presented identification systems. The presented topic of the paper has potential practical use.

In the future, the authors will analyse other acoustoelectronic components and signals. There is an idea to analyse: other acoustic signals (Lara *et al.*, 2015), acoustic holography (Jozwik, 2016), vibrations (Li *et al.*, 2016; 2017; Krolczyk *et al.*, 2014; Sawczuk, 2017; Sawczuk, Szymanski, 2017), and application of signals for power electronics (Spanik *et al.*, 2013; Frivaldsky *et al.*, 2013).

Acknowledgments

This work was supported by the Grant Agency VEGA from the Ministry of Education of Slovak Republic under contract 1/0602/17 and project No. ITMS 26220120046.

The authors thank unknown reviewers for their valuable suggestions.

Conflicts of Interest

The authors declare no conflict of interest.

References

1. Alshaykh M.S. *et al.* (2017), *High-speed stimulated hyperspectral Raman imaging using rapid acousto-optic delay lines*, Optics Letters, **42**, 8, 1548–1551, http://dx.doi.org/10.1364/OL.42.001548.
2. Audier X., Balla N., Rigneault H. (2017), *Pump-probe micro-spectroscopy by means of an ultra-fast acousto-optics delay line*, Optics Letters, **42**, 2, 294–297, http://dx.doi.org/10.1364/OL.42.000294.
3. Cho Y., Kumar A., Xu S., Zou J. (2017), *Micromachined silicon acoustic delay line with improved structural stability and acoustic directivity for real-time photoacoustic tomography*, Photons Plus Ultrasound: Imaging and Sensing 2017, Book Series: Proceedings of SPIE, Vol. 10064, Article Number: UNSP 100645E.
4. Djoumi L. *et al.* (2016), *New optical approach of SAW delay line characterization*, Proceedings of the 30th Anniversary Eurosensors Conference – Eurosensors 2016, Book Series: Procedia Engineering, **168**, 838–843, http://dx.doi.org/10.1016/j.proeng.2016.11.286.
5. Fang C., Ustun A., Cho Y., Zou J. (2017), *A charge amplification approach for photoacoustic tomography (PAT) with parallel acoustic delay line (PADL) arrays*, Measurement Science and Technology, **28**, 5, https://doi.org/10.1088/1361-6501/aa6367.
6. Frivaldsky M., Drgona P., Spanik P. (2013), *Experimental analysis and optimization of key parameters of ZVS mode and its application in the proposed LLC converter designed for distributed power system application*, International Journal of Electrical Power & Energy Systems, **47**, 448–456.
7. Gruber C., Binder A., Lenzhofer M. (2016), *Fast phase analysis of SAW delay lines*, Internet of Things: IOT Infrastructures, IOT 360, Pt II, Book Series: Lecture Notes of the Institute for Computer Sciences Social Informatics and Telecommunications Engineering, **170**, 373–382, https://doi.org/10.1007/978-3-319-47075-7_42.
8. Hartmann C.S. (1985), *Future high volume applications of SAW devices*, IEEE Ultrasonic Symposium, San Francisco, CA, USA.
9. Hasanov A.R., Hasanov R.A. (2017), *Some peculiarities of the construction of an acousto-optic delay line with direct detection*, Instruments and Experimental Techniques, **60**, 5, 722–724, http://dx.doi.org/10.1134/S0020441217050062.
10. Jozwik J. (2016), *Identification and monitoring of noise sources of cnc machine tools by acoustic holography methods*, Advances in Science and Technology-Research Journal, **10**, 30, 127–137, http://dx.doi.org/10.12913/22998624/63386.
11. Kim J., Kim S., Lee K. (2017), *Development of wireless, chipless neural stimulator by using one-port surface acoustic wave delay line and diode-capacitor interface*, Japanese Journal of Applied Physics, **56**, 6, http://dx.doi.org/10.7567/JJAP.56.06GN13.
12. Krolczyk G.M., Krolczyk J.B., Legutko S., Hunjet A. (2014), *Effect of the disc processing technology on the vibration level of the chipper during operations*, Tehnicki Vjesnik-Technical Gazette, **21**, 2, 447–450.
13. Lara R., Jimenez-Romero R., Perez-Hidalgo F., Redel-Macias M.D. (2015), *Influence of constructive parameters and power signals on sound quality and airborne noise radiated by inverter-fed induction motors*, Measurement, **73**, 503–514, http://dx.doi.org/10.1016/j.measurement.2015.05.049.
14. Li Z., Jiang Y., Hu C., Peng Z. (2016), *Recent progress on decoupling diagnosis of hybrid failures in gear transmission systems using vibration sensor signal: a review*, Measurement, **90**, 4–19, http://dx.doi.org/10.1016/j.measurement.2016.04.036.
15. Li Z., Jiang Y., Hu C., Peng Z. (2017), *Difference equation based empirical mode decomposition with application to separation enhancement of multi-fault vibration signals*, Journal of Difference Equations and Applications, **23**, 1–2, 457–467, http://dx.doi.org/10.1080/10236198.2016.1254206.
16. Lukyanov D., Shevchenko S., Kukaev A., Safronov D. (2017), *Experimental study of laser trimmed surface acoustic wave delay line topologies*, Optical Sensors 2017, Book Series: Proceedings of SPIE, **10231**, Article Number: UNSP 102311T, http://dx.doi.org/10.1117/12.2265675.
17. Marzo A., Ghobrial A., Cox L., Caleap M., Croxford A., Drinkwater B.W. (2017), *Realization of compact tractor beams using acoustic delay-lines*, Applied Physics Letters, **110**, 1, Article Number: 014102, http://dx.doi.org/10.1063/1.4972407.
18. Neveselý M. (1986), *Akustoelektronika*, Bratislava, ALFA.

19. Ruppel C.C.W., Fjeldy T.A. (2000), *Advances in SAW Technology Systems and Applications*, World Scientific, Singapore.

20. Sawczuk W. (2017), *The application of vibration accelerations in the assessment of average friction coefficient of a railway brake disc*, Measurement Science Review, **17**, 3, 125–134, http://dx.doi.org/10.1515/msr-2017-0016.

21. Sawczuk W., Szymanski G.M. (2017), *Diagnostics of the railway friction disc brake based on the analysis of the vibration signals in terms of resonant frequency*, Archive of Applied Mechanics, **87**, 5, 801–815.

22. Spanik P., Sedo J., Drgona P., Frivaldsky M. (2013), *Real time harmonic analysis of recuperative current through utilization of digital measuring equipment*, Elektronika ir Elektrotechnika, **19**, 5, 33–38.

23. Tung P.-H., Wang W.-C., Yang C.-H. (2015), *A study in wedge waves with applications in acoustic delay-line*, Proceedings of the 2015 ICU International Congress on Ultrasonics, Book Series: Physics Procedia, **70**, 199–203, http://dx.doi.org/10.1016/j.phpro.2015.08.122.

24. Zhang B., Hu H. (2015), *A FEM simulation approach for multilayered SAW delay line devices*, IEEE International Conference on Robotics and Biomimetics (ROBIO), 970–975.

25. Zheng Z., Han T., Qin P. (2015), *Maximum measurement range and accuracy of SAW reflective delay line sensors*, Sensors, **15**, 10, 26643–26653, http://dx.doi.org/10.3390/s151026643.

26. Zhu H.S., Rais-Zadeh M. (2017), *Non-reciprocal acoustic transmission in a GaN delay line using the acoustoelectric effect*, IEEE Electron Device Letters, **38**, 6, 802–805, http://dx.doi.org/10.1109/LED.2017.2700013.